ARTICLE

Synthesis and Magnetic Properties of Co_3O_4 Nanoflowers

Yuan-guang Zhang*, You-cun Chen, Yin-guo Zhao

Department of Chemistry, Anqing Normal College, Anqing 246011, China

(Dated: Received on March 9, 2007; Accepted on August 2, 2007)

Co_3O_4 nanoflowers were prepared through a sequential process of a hydrothermal reaction and heat treatment. The as-synthesized products were characterized by powder X-ray diffraction, field-emission scanning electron microscopy, transmission electron microscopy, and infrared spectrum. These nanoflowers consist of numerous Co_3O_4 nanofibers, which have diameters of 20-40 nm, and lengths ranging from 100 nm to 500 nm. They have pore structures and Brunauer-Emmett-Teller surface area of ∼34.61 m^2/g. The temperature dependence curves of magnetization in zero-field-cooled conditions and field-cooled indicate mainly antiferromagnetism and weak ferromagnetism of Co_3O_4 nanoflowers at blocking temperature of ∼34 K respectively.

Key words: Co_3O_4, Synthesis, Magnetic properties, Nanoflowers

I. INTRODUCTION

Magnetic nanoparticles are of great importance as they are potential materials for applications in varied fields. The size reduction of a magnetic material leads to novel properties such as superparamagnetism [1]. That is, with decreasing particle size, the magnetic anisotropy energy per particle responsible for holding the magnetic moment along certain directions becomes comparable to thermal energy. The thermal energy will then induce random flipping of the magnetic moment with time and the magnetic particles will lose their magnetic order. Another property that arises from size reduction is spin canting [2,3], where the spin structure of the particles is noncollinear, with the spins inclined at an angle to their normal direction due to competing antiferromagnetic exchange interactions at the surfaces of the particles.

Four decades ago, Néel predicted antiferromagnetic nanoparticles (AFNs) would exhibit induced permanent magnetic moments due to the lack of internal structural perfection and/or uncompensated spins on the surface of the particles [4]. Below a critical temperature and particle size, uncompensated spins in AFNs may give rise to a superparamagnetic relaxation of their spin lattices [1]. It is well known that Co_3O_4 has a normal spinel structure and bulk Co_3O_4 exhibits antiferromagnetism with the Néel temperature at around 30 K [5]. The Co^{3+} ($3d^6$) at the octahedral sites are diamagnetic in the octahedral crystal field. The Co^{2+} at the tetrahedral sites form an antiferromagnetic sublattice with the diamond structure below the Néel temperature. Therefore, Co_3O_4 has gained increased attention for exhibiting quantum tunneling of magnetization [6,7]. The Co_3O_4 nanoparticle system has also been used in the study of macroscopic magnetic quantum effects and for the production of a mesoporous metal oxide framework structure by nanocasting means employing vinyl-functionalized silica as a template [8,9]. The effect on Co_3O_4 magnetic properties has been investigated according to the changing conditions (size [9], temperature [9-11], diluted [11], magnetic field and frequency [8]). Hence research on synthesis and magnetic studies of Co_3O_4 nanoparticles of desired size and shape has become significant.

Co_3O_4 with different structures have been studied [12] due to their wide applications in magnetic materials [13], gas sensors [14], catalysts [15], electrochromic devices [16], and high-temperature solar selective absorbers [17]. Usually, transition metal spinels are conventionally synthesized by a solid-state reaction of mixed metal salts at elevated temperatures. However, extremely active atomic vibration at high reaction temperature usually leads to sintering and/or grain growth, unlikely to produce nanoparticles. Many techniques have been devised for the low-temperature synthesis of transition metal spinel. For example, single-phase Co_3O_4 at temperatures ranging from 150 °C to 260 °C has been made via spray pyrolysis, chemical vapor deposition, and sol-gel routes [18-20]. Co_3O_4 could be formed at 70-100 °C from a precursor compound cobalt (III) hydroxyoxide (CoOOH) [21-23]. Monodispersed 100-nm Co_3O_4 nanocubes has been prepared by means of a traditional forced hydrolysis method [24]. Spinel oxide cubes with a dimensional scale of 10-100 nm have been obtained through a salt-mediated preparation process, in which the size and shape controls was attributed to a salt-(solvent) diffusion boundary coating the surfaces of the resulting Co_3O_4 nanoparticles [25]. Xu and Zeng synthesized Co_3O_4 nanocubes smaller than 10 nm and their superstructures by adding capping agent Tween-85 into their reaction system [26]. Co_3O_4 rods consisting of nanoparticles had been prepared by

*Author to whom correspondence should be addressed. E-mail: ygz@aqtc.edu.cn

thermal decomposition of cobalt oxalate nanorods [27]. In addition, Co_3O_4 nanorods have been synthesized at 160 °C for 10 h by a solvothermal method [28]. Co_3O_4 nanosheets have been synthesized by hydrothermal oxidation of the layered precursor Co(II) acetate hydroxide using H_2O_2 [29]. Co_3O_4 hollow spheres were hydrothermally prepared at 130 °C for 16 h in the presence of Poly-vinylpyrrolidone (PVP) [30]. Cobalt oxide (Co_3O_4) flowers have been obtained by thermal decomposition of cobalt hydroxide flowers in air at 400 °C [31].

To the best of our knowledge, porous Co_3O_4 nanomaterials are seldom reported. Schuth *et al.* synthesized mesoporous Co_3O_4 by nanocasting process [9]. Li *et al.* prepared mesoporous Co_3O_4 nanocrystals [32]. Wang *et al.* synthesized porous Co_3O_4 nanotubes through a modified microemulsion method [33]. The concept of utilizing mesoporous silica phases as rigid structure matrices [34,35] has extended the opportunities to create new ordered mesoporous metal oxides which were formerly not available, including In_2O_3, Co_3O_4, Cr_2O_3, Mn_xO_y, NiO, and Fe_2O_3 [36-41]. In this procedure, the pores of the solid structure matrix are filled with a precursor, which is then converted *in situ* to the respective metal oxide, then the structure matrix is finally removed. This type of synthesis allows for much higher reaction temperatures than the conventional method of supramolecular structure direction. The structure matrix serves as a rigid skeleton, allowing for the metal oxide to crystallize without loss of the nanostructural periodic order. Mesoporous SBA-15 and KIT-6 silica materials have successfully been used as structure matrices for the synthesis of mesoporous CeO_2 [42-44].

In this work, nanoporous Co_3O_4 hierarchical nanoflowers were prepared through a sequential process of a hydrothermal reaction and heat treatment. The temperature dependences of as-obtained flower-like Co_3O_4 nanoparticles magnetization in zero-field-cooled (ZFC) and field-cooled (FC) formation conditions exhibit antiferromagnet and weak ferromagnetic properties, respectively. Their blocking temperatures are obviously related to their sizes. Moreover, the optic property of as-obtained flower-like Co_3O_4 nanoparticles displays their quantum-confined effect.

II. EXPERIMENTS

A. Synthesis of Co_3O_4 nanoflowers

In a typical procedure, 1 mmol $Co(NO_3)_2$ and 5 mmol $CO(NH_2)_2$ were dissolved in 40 mL distilled water to form a pink homogeneous solution under stirring, and then the solution was transferred to 50 mL Teflon liner. After that, the liner was sealed in a stainless steel autoclave, maintained at 90 °C for 10 h, and then allowed to cool to room temperature naturally. The precipitate obtained was heated at 300 °C for 3 h. Finally, the Co_3O_4 nanoflowers were obtained.

B. Characterization of Co_3O_4 nanoflowers

The products were characterized by powder X-ray diffraction (XRD, Rigaku D with Cu Kα_1 radiation wavelength λ=1.5418 Å), infrared spectrum (IR) recorded on a Bruker Vector-22 FT-IR sepectrometer from 400 cm^{-1} to 4000 cm^{-1} at room temperature on KBr mulls. scanning electron microscopy (SEM, HITACHIX-650 and JEOL JSM-6700F), transmission electron microscopy (TEM, JEOL 2010 using an accelerating voltage of 200 kV), nitrogen adsorption-desorption curve (Barret Emmett Teller surface area, Micromeritics ASAP 2010 system), magnetic measurements (a SQUID magnetometer, Quantum Design MPMS), and ultraviolet and visible spectra (JGNA Specord 200 PC UV-visible spectrophotometer). The samples used for characterization were dispersed in absolute ethanol and were ultrasonicated before SEM and TEM observation.

III. RESULTS AND DISCUSSION

Figure 1 shows the XRD pattern of as-obtained products. All the peaks can be indexed to cubic phase Co_3O_4 (Fd3m) with lattice parameter a=8.089 Å, which is close to the reported value (a=8.083 Å) (JCPDS: 76-1802). No other peaks of impurities can be detected. Estimated according to Debey-Scherrer formula, the average particle size is ∼11 nm.

Figure 2 shows the XPS spectra of the final products. The Co2p binding energies are 780.2 and 795.3 eV, respectively. The O1s binding energy is 530.06 eV. The molar ratio of Co to O quantified by Co2p and O1s peak area, is close to 3:4, approaching the stoichiometry of Co_3O_4.

Figure 3 shows the IR spectrum of the final products. The IR absorption peaks at about 663.72 and

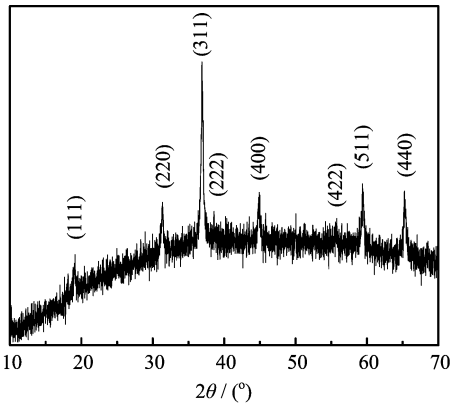

FIG. 1 A typical XRD pattern of as-obtained products.

DOI:10.1088/1674-0068/20/05/601-606

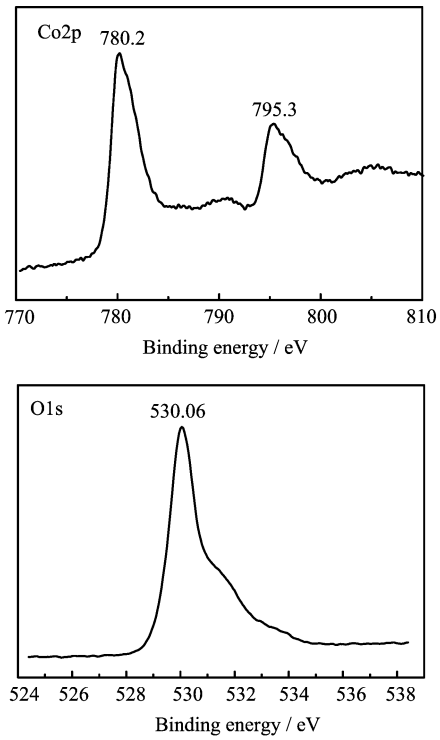

FIG. 2 The XPS spectra of as-obtained products.

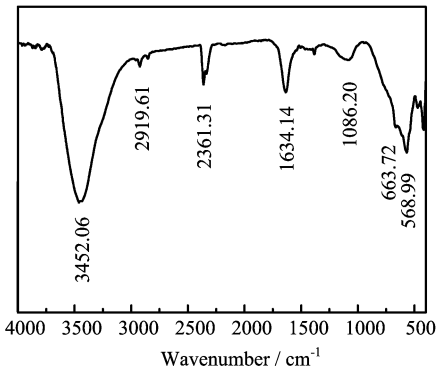

FIG. 3 The IR spectrum of as-obtained products.

568.99 cm^{-1} confirm the formation of the phase of spinel Co_3O_4 [45]. The broad band centered at about 3452.06 cm^{-1} and peak at 1634.14 cm^{-1} are assigned to the O−H stretching and bending modes of water [46]. The IR and XPS analysis further confirmed that the as-prepared products are Co_3O_4 phase, which is in agreement with analysis result of XRD.

Figure 4(a) shows sphere-like products. The Co_3O_4 nanoflowers have diameters of 500-1000 nm. Magnified FE-SEM image of single Co_3O_4 product (inset in Fig.4(a)) indicates that as-obtained Co_3O_4 looks like flowers on the whole, and the units composing the structure loosely radiate from the center. Closer observations are focusing on the surface of nanoflowers. Figure 4(b) reveals the microstructure of these units. These units

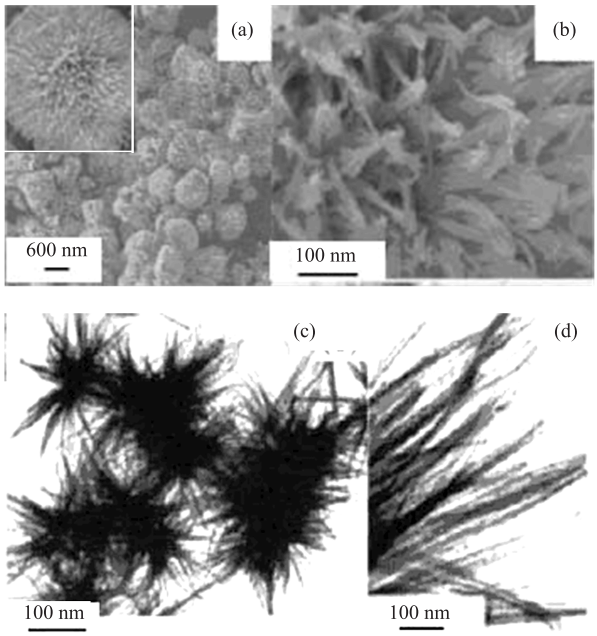

FIG. 4 (a) Low-magnification (inset: single Co_3O_4 nanoflower) and (b) high-magnification FE-SEM images of as-obtained Co_3O_4 nanoflowers. (c) and (d) the whole and part TEM images of Co_3O_4 nanoflowers, respectively.

consist of large amounts of nanofiber bundles. Each bundle exhibits a dandelion-like shape, and nanofibers in bundles connect to each other. Figure 4 (c) and (d) show TEM images of the products. The Co_3O_4 nanofibers have diameters of 20-40 nm, and lengths ranging from 100 nm to 500 nm. Enlarged TEM images in Fig.4(d) confirm that these nanofibers are made up of a great deal of nanoparticles with an average size of ∼11 nm. The results are identical to the XRD results.

Figure 5(a) shows representative nitrogen adsorption/desorption isotherms of Co_3O_4 nanoflowers and the corresponding Barrett-Joyner-Halenda (BJH) pore size distribution curve of Co_3O_4 nanoflowers are shown in Fig.5(b). The nitrogen isotherm of the products is a type IV isotherm with a similar H1-type hysteresis loop, indicating Co_3O_4 nanoflowers consist of an almost uniform mesoporous texture. The as-obtained Co_3O_4 nanoflowers have a BET surface area of ∼34.61 m^2/g. The BJH analyses show that Co_3O_4 nanoflowers possess bimodal (small and large) mesopore distribution, which is a unique characterization of as-obtained porous Co_3O_4 nanoflowers. This result is different from the previous report of mesoporous Co_3O_4 [9]. Figure 5(b) displays main pore size distribution of ∼9 nm (small pore) in as-obtained nanoflowers. The small pores exist in all mesoporous nanofibers composing Co_3O_4 nanoflowers. The result is in good agreement with the value determined by the above FE-SEM and TEM observations. Another larger pore size distribution of ∼29 and 52 nm are mainly formed by the aggregation of the nanofibers, that is, the interspace in Co_3O_4

DOI:10.1088/1674-0068/20/05/601-606

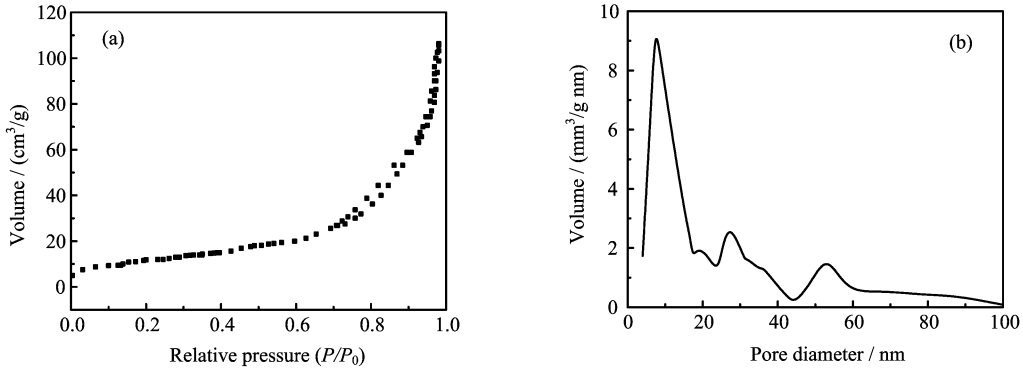

FIG. 5 N_2 adsorption-desorption isotherm of the nanoporous Co_3O_4 nanoflowers (a), and pore-size distribution curve obtained from the desorption data (b).

nanoflowers. The hierarchical structures with smaller and larger mesopores could reduce transport limitation in catalysis, resulting in higher activities and well-controlled selectivities [47]. The bimodal mesoporous Co_3O_4 nanoflowers may have promising applications in catalysis since their larger textural mesopores can provide reactant substances of different size transport circumstance comparable to those in open medium [48].

As is well known, the physical properties of materials are closely related to their structures and morphologies. This aspect is more obvious in nanomaterials than in bulk materials. In order to investigate the magnetic behavior of nanoporous Co_3O_4 nanoflowers, the temperature dependences of magnetization in ZFC and FC conditions were carried out (Fig.6). The ZFC curve mainly shows the antiferromagnetism of as-obtained products. However, this ZFC curve has a remarkable feature: the broad peak at ∼34 K with a full width >47 K, suggesting that nanoporous Co_3O_4 nanoflowers have weak ferromagnetic behavior at low temperature. This is similar to the report about mesoporous Co_3O_4 [9]. The ferromagnetic ordering of excess surface spins in nanomaterials may contribute to the weak ferromagnetism in antiferrimagnetic materials. ZFC and FC curves have similar linetype, and FC magnetization is always slightly higher than ZFC's from 4 K to 300 K. It is obviously different from ZFC and ZF magnetization of Co_3O_4 nanoparticles [49]. All the differences should be related to the unique structure of as-obtained Co_3O_4 nanoflowers, such as relative high BET surface area, different kinds of mesopores, and hierarchical morphology. In addition, the blocking temperature (34 K) observed in this experiment is lower than that (40 K) for Co_3O_4 nanocystals with average size of ∼7 nm [26], but higher than 25 K for Co_3O_4 nanoparticles with size of ∼20 nm [50]. It is likely that smaller Co_3O_4 nanooparticles with higher surface-to-volume ratio exhibit much larger proportion of noncompensated surface spins on the antiferromagnetic core and thus reveal higher blocking temperature. Similarly, the smaller average particle size, which corresponds to a higher fraction of surface spins, and hence for which bulk behavior is expected to occur at higher temperature. A similar phenomenon can been found in previous literature, reporting blocking temperature increase with decreasing particle size [50].

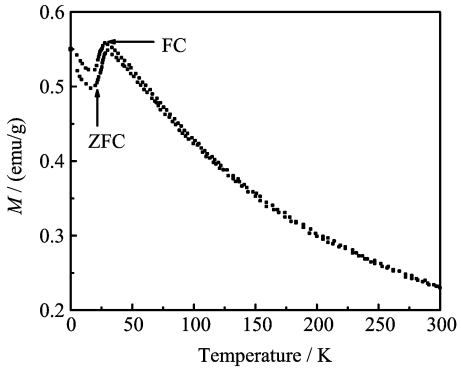

FIG. 6 Magnetization for FC and ZFC Co_3O_4 nanoflowers in 1.0 T applied field as a function of temperature.

The optical absorption property of as-obtained Co_3O_4 nanoflowers is investigated at room temperature by UV-Visible spectroscopy (Fig.7). There are two obvious absorption peaks (λ∼720 nm and λ<500 nm) in Fig.7(a), which indicate ligand-metal charge transfer events O(-II)→Co(II) and O(-II)→Co(II), respectively [51]. Co_3O_4 is a p-type semiconductor and its optical band gap can be obtained by the following equation:

$$(\alpha h\nu)^n = B(h\nu - E_g) \quad (1)$$

where α is the absorption coefficient, $h\nu$ is the photo energy, B is a constant relative to the material, E_g is the band gap, and n is either 1/2 for an indirect transition or 2 for a direct transition. The $(\alpha h\nu)^2$-$h\nu$ curve for the products is shown in Fig.7(b), exhibiting two plots of linear relationship at 2.15-2.45 and 1.52-1.62 eV. The band gaps of as-obtained Co_3O_4 are 1.98 and 1.49 eV by Eq.(1), revealing obvious blue shift in comparison with the previous report [52]. This shift may be caused by the small size (only 10 nm) of nanoparticles composing

DOI:10.1088/1674-0068/20/05/601-606

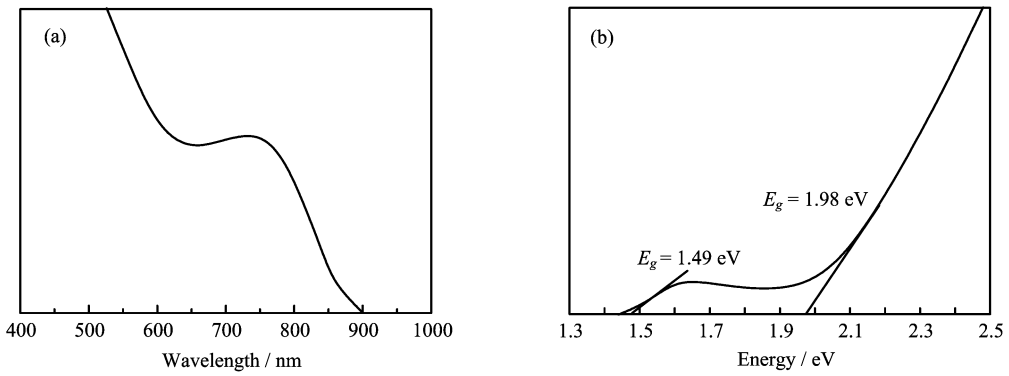

FIG. 7 (a) UV-Vis spectrum of Co_3O_4 nanoflowers. (b) Spectrum obtained by using the energy as abscissa.

of Co_3O_4 nanoflowers, suggesting the quantum confined effect and semiconductor traits. Here, the valence band has a strong O2p character, while the main contribution to the conduction band is given by the Co(II) 3d orbital. The presence of Co(III) centers in Co_3O_4 gives rise to a subband located inside the energy gap. Hence, 1.49 eV corresponds to the onset of O (-II)→Co(III) excitations, while 1.98 eV is the "true" energy gap corresponding to interband transitions. In addition, it can be found that the best fitting of Eq.(1) to the absorption spectra of the products gives n=2, suggesting that the as-obtained Co_3O_4 nanoflowers possess a semiconductor trait with direct transitions to these energies.

IV. CONCLUSION

In conclusion, hierarchical Co_3O_4 nanoporous nanoflowers were synthesized via a sequential process of a hydrothermal reaction and heat treatment. Co_3O_4 nanoflowers have two kinds of pore structures (small pore size distribution of ∼9 nm and large pore size distribution of ∼29 and 52 nm). The bimodal pore structure may have promising applications in catalysis owing to reducing transport limitation in catalysis, resulting in higher activities and well-controlled selectivities. The temperature dependences of magnetization in ZFC and FC conditions indicate the mainly antiferromagnetic and weak ferromagnetic properties of Co_3O_4 nanoflowers, respectively. In addition, the optic property of as-obtained product obviously indicates a blue shift of band gaps, suggesting the quantum-confined effect and traits of a semiconductor.

V. ACKNOWLEDGMENT

This work was supported by the National Natural Science Foundation of China (No.20371002).

[1] S. Chikazumi, *Physics of Ferromagnetism*, New York: Oxford University Press, (1997).
[2] B. Martinez, X. Obradors, L. Balcells, A. Rouanet, and C. Monty, Phys. Rev. Lett. **80**, 181 (1998).
[3] R. H. Kodama, A. E. Berkowitz, E. J. McNiff, and S. Foner, Mater. Sci. Forum **643**, 235 (1997).
[4] L. Néel, *In Low-Temperature Physics*, C. Dewitt, B. Dreyfus, and P. D. de Gennes, Eds., New York: Gordon and Breach, 413 (1962).
[5] W. Kundig, M. Kobelt, H. Appel, G. Constabaris, and R. H. Lindequist, J. Phys. Chem. Solids **30**, 819 (1969).
[6] A. O'Caldera and A. Legget, J. Phys. Rev. Lett. **46**, 211 (1981).
[7] E. M. Chudnovsky, J. Appl. Phys. **73**, 6697 (1993).
[8] S.Takada, M. Fujii, S. Kohiki, T. Babasaki, H. Deguchi, M. Mitome, and M. Oku, Nano. Lett. **1**, 379 (2001).
[9] Y. Q. Wang, C. M. Yang, W. G. Schmidt, B. Spliethoff, E. Bill, and F. Schuth, Adv. Mater. **17**, 53 (2005).
[10] M. Sato, S. Kohiki, Y. Hayakawa, Y. Sonda, T. Babasaki, H. Deguchi, and M. Mitome, J. Appl. Phys. **88**, 2771 (2000).
[11] Y. Hayakawaa, S. Kohikia, M. Satoa, Y. Sonda, T. Babasaki, H. Deguchi, A. Hidaka, H. Shimooka, and S. Takahashi, Physica E **9**, 250 (2001).
[12] (a) X. Y. Shi, S. Han, R. J. Sanedrin, C. Galvez, D. G. Ho, F. Zhou, and M. Selke, Nano. Lett. **2**, 289 (2002).
(b) T. He, D. R. Chen, and X. L. Jiao, Chem. Mater. **16**, 737 (2004).
[13] M. T. Verelst, O. Ely, C. Amiens, E. Snoeck, P. Lecante, A. Mosset, M. Respaud, J. M. Brotom, and B. Chaudret, Chem. Mater. **11**, 2702 (1999).
[14] (a) M. Andok, T. Kobayashi, S. Iijima, and M. Haruta, J. Mater. Chem. **7**, 1779 (1997).
(b) H. Yamaura, J. Tamaki, K. Moriya, N. Miura, and N. Yamazoe, J. Electrochem. Soc. **144**, L158 (1997).
[15] (a) P. Nkeng, J. Koening, J. Gautier, P. Chartier, and G. Poillerat, J. Electroanal. Chem. **402**, 81 (1996).
(b) S. G. Chrisoskova, M. Stoyanova, M. Georgieva, and D. Mehandjiev, Mater. Chem. Phys. **60**, 39 (1999).
(c) M. M. Natile and A. Glisenti, Chem. Mater. **14**, 3090 (2002).
[16] T. Maruyama and S. Arai, J. Electrochem. Soc. **143**, 1383 (1996).
[17] (a) G. B. Smith, A. Ignatiev, and G. Zajac, J. Appl.

DOI:10.1088/1674-0068/20/05/601-606

Phys. **51**, 4186 (1980).
(b) K. Chidambaram, K. L. Malhotra, and K. L. Chopra, Thin Solid Films **87**, 365 (1982).
[18] M. E. Baydi, G. Poillerat, J. L. Rehspringer, J. L. Gautier, J. F. Koenig, and P. Chartier, J. Solid State Chem. **109**, 281 (1994).
[19] E. Fujii, H. Torii, A. Tomozawa, R. Takayama, and T. Hirao, J. Mater. Sci. **30**, 6013 (1995).
[20] J. L. Gautier, E. Rios, M. Gracia, J. F. Marco, and J. R. Gancedo, Thin Solid Films **311**, 51 (1997).
[21] T. Sugimoto and E. Matijevic, J. Inorg. Nucl. Chem. **41**, 165 (1978).
[22] R. M. Rojas, E. Vila, O. Garcia, and J. L. Martin de Vidales, J. Mater. Chem. **4**, 1635 (1994).
[23] G. Furlanetto and L. Formado, J. Colloid Interface Sci. **170**, 169 (1995).
[24] T. Sugimoto and E. Matijevi'c, J. Inorg. Nucl. Chem. **41**, 165 (1979).
[25] J. Feng and H. C. Zeng, Chem. Mater. **15**, 2829 (2003).
[26] N. R. Jana, Y. Chen, and X. Peng, Chem. Mater. **16**, 3931 (2004).
[27] W. W. Wang and Y. J. Zhu, Mater. Res. Bull. **40**, 1929 (2005).
[28] Y. C. Chen and Y. G. Zhang, Chin. J. Chem. Phys. **17**, 481 (2004).
[29] Z. H. Liang, Y. J. Zhu, G. F. Cheng, and Y. H. Huang, Can. J. Chem. **84**, 1050 (2006).
[30] Y. C. Chen, Y. G. Zhang, and S. Q. Fu, Mater. Lett. **61**, 701 (2007).
[31] L. X. Yang, Y. J. Zhu, L. Li, L. Zhang, H. Tong, W. W. Wang, G. F. Cheng, and J. F. Zhu, Eur. J. Inorg. Chem. **23**, 4787 (2006).
[32] L. Cao, M. Lu, and H. L. Li, J. Electrochem. Soc. **152**, A871 (2005).
[33] R. M. Wang, C. M. Liu, H. Z. Zhang, C. P. Chen, L. Guo, H. B. Xu, and S. H. Yang, Appl. Phys. Lett. **85**, 2080 (2004).
[34] A. H. Lu and F. Schuth, Adv. Mater. **18**, 1793 (2006).
[35] Y. Wan, H. Yang, and D. Zhao, Acc. Chem. Res. **39**, 423 (2006).
[36] B. Tian, X. Liu, H. Yang, S. Xie, C. Yu, B. Tu, and D. Zhao, Adv. Mater. **15**, 1370 (2003).
[37] H. Yang, Q. Shi, B. Tian, Q. Lu, F. Gao, S. Xie, J. Fan, C. Yu, B. Tu, and D. Zhao, J. Am. Chem. Soc. **125**, 4724 (2003).
[38] J. H. Smatt, B. Spliethoff, J. B. Rosenholm, and M. Lindén, Chem. Commun. 2188 (2004).
[39] J. H. Smatt, C. Weidenthaler, J. B. Rosenholm, and M. Lindén, Chem. Mater. 1443 (2006).
[40] F. Jiao, A. Harrison, J. C. Jumas, A. V. Chadwick, W. Kockelmann, and P. G. Bruce, J. Am. Chem. Soc. **128**, 5468 (2006).
[41] C. Dickinson, W. Zhou, R. P. Hodgkins, Y. Shi, D. Zhao, and H. He, Chem. Mater. **18**, 3088 (2006).
[42] S. C. Laha and R. Ryoo, Chem. Commun. 2138 (2003).
[43] E. Rossinyol, J. Arbiol, F. Peiro, A. Cornet, J. R. Morante, B. Tian, T. Bo, and D. Zhao, Sens. Actuators B **109**, 57 (2005).
[44] W. Shen, X. Dong, Y. Zhu, H. Chen, and J. Shi, Micropor. Mesopor. Mater. **85**, 157 (2005).
[45] J. A. Gaddsden, *Infrared Spectra of Minerals and Related Inorganic Compounds*, London: Butterworth, 44 (1975).
[46] K. Nakamoto, *Infrared Spectra of Inorganic and Coordination Compound*, Translated by D. Huang and R. Wang, Beijing: 4th Chemical Industry Press, 251 (1991).
[47] (a) T. R. Liu, Y. Pinnavaia, J. L. Billinge, and T. P. Bieker, J. Am. Chem. Soc. **121**, 8835 (1999).
(b) L. Z. Zhang and J. C. Yu, Chem. Commun. 2078 (2003).
(c) S. T. Wong, H. P. Lin, and C. Y. Mou, Appl. Catal. A **198**, 103 (2000).
[48] D. R. Rolison, Science **299**, 1698 (2003).
[49] S. A. Makhlouf, J. Magn. Magn. Mater. **246**, 184 (2002).
[50] (a) T. Hyeon, S. S. Lee, J. Park, Y. Chung, and H. B. Na, J. Am. Chem. Soc. **123**, 12798 (2001).
(b) W. S. Seo, H. H. Jo, K. Lee, B. Kim, S. J. Oh, and J. T. Park, Angew. Chem. Int. Ed. **43**, 1115 (2004).
[51] (a) I. D. Belova, Y. E. Roginskaya, R. R. Shifrina, S. G. Gagarin, Y. V. Plekhanov, and Y. N. Venevtsev, Solid State Commun. **47**, 577 (1983).
(b) J. G. Cook and M. P. van Der Meer, Thin Solid Films **144**, 165 (1986).
[52] (a) X. Wang, X. Y. Chen, L. S. Gao, H. G. Zheng, Z. D. Zhang, and Y. T. Qian, J. Phys. Chem. B **108**, 16401 (2004).
(b) D. Barreca, C. Massign, S. Daolio, M. Fabrizio, C. Piccirillo, L. Armelao, and E. Tondello, Chem. Mater. **13**, 588 (2001).
(c) T. Maruyama and T. Nakai, Sol. Energy Mater. **23**, 25 (1991).
(d) C. S. Cheng, M. Serizawa, H. Sakata, and T. Hirayama, Mater. Chem. Phys. **53**, 225 (1998).
(e) P. S. Patil, L. D. Kadam, and C. D. Lokhande, Thin Solid Films **272**, 29 (1996).

DOI:10.1088/1674-0068/20/05/601-606